

Research



**Cite this article:** Van Bruggen S *et al.* 2023

Neutrophil peptidylarginine deiminase 4 is essential for detrimental age-related cardiac remodelling and dysfunction in mice. *Phil. Trans. R. Soc. B* **378**: 20220475.

*Phil. Trans. R. Soc. B* **378**: 20220475.

<https://doi.org/10.1098/rstb.2022.0475>

Received: 11 April 2023

Accepted: 21 June 2023

One contribution of 16 to a Theo Murphy meeting issue ‘The virtues and vices of protein citrullination’.

**Subject Areas:**

physiology

**Keywords:**

citrullination, neutrophils, cardiac ageing, fibrosis

**Author for correspondence:**

Kimberly Martinod

e-mail: kim.martinod@kuleuven.be

Electronic supplementary material is available online at <https://doi.org/10.6084/m9.figshare.c.6806584>.

# Neutrophil peptidylarginine deiminase 4 is essential for detrimental age-related cardiac remodelling and dysfunction in mice

Stijn Van Bruggen<sup>1</sup>, Sirima Kraisin<sup>1</sup>, Jore Van Wauwe<sup>1</sup>, Katrien Bomhals<sup>1</sup>, Mathias Stroobants<sup>1</sup>, Paolo Carai<sup>1</sup>, Liesbeth Frederix<sup>1</sup>, Alexander Van De Bruaene<sup>2,3</sup>, Thilo Witsch<sup>4</sup> and Kimberly Martinod<sup>1</sup>

<sup>1</sup>Center for Molecular and Vascular Biology, Department of Cardiovascular Sciences, KU Leuven, O&N1 Herestraat 49 - Bus 911, 3000 Leuven, Belgium

<sup>2</sup>Division of Cardiology, Department of Cardiovascular Sciences, KU Leuven, KU Leuven, Leuven 3000, Belgium

<sup>3</sup>Division of Structural and Congenital Cardiology, University Hospitals Leuven, Leuven 3000, Belgium

<sup>4</sup>Department of Cardiology and Angiology I, University of Freiburg, Heart Center, Faculty of Medicine, University of Freiburg, Freiburg 79110, Germany

**ID** SVB, 0000-0002-5572-2196; SK, 0000-0003-4836-9387; JWV, 0000-0003-2969-1805; KB, 0000-0003-1170-484X; MS, 0009-0004-7018-3081; PC, 0000-0003-0718-4773; AVDB, 0000-0002-0469-8640; TW, 0000-0003-4003-1269; KM, 0000-0002-1026-6107

Mice fully deficient in peptidylarginine deiminase 4 (PAD4) enzyme have preserved cardiac function and reduced collagen deposition during ageing. The cellular source of PAD4 is hypothesized to be neutrophils, likely due to PAD4's involvement in neutrophil extracellular trap release. We investigated haematopoietic PAD4 impact on myocardial remodelling and systemic inflammation in cardiac ageing by generating mice with *Padi4* deletion in circulating neutrophils under the MRP8 promoter (Ne-PAD4<sup>-/-</sup>), and ageing them for 2 years together with littermate controls (PAD4<sup>fl/fl</sup>). Ne-PAD4<sup>-/-</sup> mice showed protection against age-induced fibrosis, seen by reduced cardiac collagen deposition. Echocardiography analysis of structural and functional parameters also demonstrated preservation of both systolic and diastolic function with MRP8-driven PAD4 deletion. Furthermore, cardiac gene expression and plasma cytokine levels were evaluated. Cardiac genes and plasma cytokines involved in neutrophil recruitment were downregulated in aged Ne-PAD4<sup>-/-</sup> animals compared to PAD4<sup>fl/fl</sup> controls, including decreased levels of C-X-C ligand 1 (CXCL1). Our data confirm PAD4 involvement from circulating neutrophils in detrimental cardiac remodelling, leading to cardiac dysfunction with old age. Deletion of PAD4 in MRP8-expressing cells impacts the CXCL1-CXCR2 axis, known to be involved in heart failure development. This supports the future use of PAD4 inhibitors in cardiovascular disease.

This article is part of the Theo Murphy meeting issue ‘The virtues and vices of protein citrullination’.

## 1. Introduction

According to projections from the World Health Organization (WHO), by 2030 one in six people will be 60 years or older. Increasing age is often accompanied by a chronic low-grade pro-inflammatory status, even in the absence of any form of infection. This state of sterile inflammation with increasing age has been defined as ‘inflammaging’ [1]. Chronic inflammation, as evaluated by plasma or serum levels of pro-inflammatory mediators, can cause malfunctioning of several cellular and molecular events, ultimately leading to various chronic ailments and diseases, as well as the loss of tissue integrity and organ function

over time [2–4], which can result in age-related pathologies, such as Alzheimer's disease, atherosclerosis, arthritis, cancer and cardiovascular diseases [5,6].

A final pathological outcome following chronic inflammation is the development of fibrosis [7]. During fibrosis development connective tissue replaces normal parenchymal tissue [8]. Even though this process initially starts off being beneficial for organ function and healing, during chronic inflammation the repair process becomes inappropriately controlled and pathogenic, resulting in substantial extracellular matrix (ECM) production and deposition, ultimately leading to the replacement of normal tissue by a fibrotic scar [9].

Fibrosis development is a complex and multi-stage process, in which bone marrow-derived leucocytes play an essential role [10]. Upon tissue injury, cells of the immune system are activated. In neutrophils, this alters the metabolic state, resulting in the release of granule proteins [11], enhanced phagocytic capabilities [12] and the production and release of reactive oxygen species (ROS) [13]. Intracellularly, ROS cause the disruption of primary granules, causing the cytoplasmic release of proteases like myeloperoxidase (MPO) and neutrophil elastase (NE) [14]. These proteins can migrate to the nucleus, with MPO facilitating the initial entry of NE into the nuclear membrane. In the nucleus, NE starts degrading histones, promoting chromatin decondensation and nuclear swelling [15]. This increase in nuclear volume continues until both nuclear and plasma membranes are incapable of resisting tensile stress, leading to cell rupture. The loss of membrane integrity is coupled with the release of nuclear material, lined with a range of proteins, including MPO, NE and histones. These extracellular DNA structures are known as neutrophil extracellular traps (NETs) [16].

The process of NET formation (also known as NETosis) often requires the activation of peptidylarginine deiminase 4 (PAD4), an enzyme involved in protein citrullination. Equipped with a nuclear localization sequence (NLS), PAD4 can citrullinate specific arginine residues on histone tails, further facilitating chromatin decondensation, which is an important stage during NETosis [17]. Although NETs were first described as an anti-bacterial defense mechanism [18,19], NETosis can also occur during sterile inflammation, as is the case during ageing [20]. Once released, NETs can cause damage to underlying tissue, and are both proinflammatory and prothrombotic [21–23]. Furthermore, NETs are released in a range of pathological conditions, including deep vein thrombosis [21,23], cancer [22,24], myocardial ischemia/reperfusion injury [25], atherosclerosis [26–28], rheumatoid arthritis [29] and other auto-immune diseases [30]. Additionally, it was shown that NETs are capable of catalyzing the conversion of fibroblasts towards collagen-secreting myofibroblasts *in vitro* [25], thus directly linking NETs to fibrosis development. However, this has not yet been demonstrated in the heart.

We have previously studied the interplay between citrullination, ageing and cardiac fibrosis by examining the effect of systemic deletion of PAD4 in aged mice [20]. This resulted in a cardioprotective phenotype with increasing age, with preservation of both systolic and diastolic function. It was shown in the same study that, with PAD4 deletion, excessive deposition of interstitial cardiac fibrosis was absent with increasing age. However, the phenotype could not be specifically attributed to neutrophils or NETs. Therefore, the overall goal of this study was to selectively knock out

PAD4 in neutrophils and to investigate how neutrophil PAD4 is mechanistically involved in the complex process of spontaneous fibrosis development with increasing age.

## 2. Material and methods

### (a) Animals and ethics statement

All experimental procedures were reviewed and approved by the Ethical Committee of the Laboratory Animal Center at the KU Leuven (Project number P019/2020), according to the Belgian Law and the guidelines from Directive 2010/63/EU of the European Parliament. B6.Cg-Pad4<sup>tm1.2K<sup>mo</sup></sup> (PAD4<sup>fl/fl</sup>, RRID IMSR\_JAX:026708) mice were purchased from the Jackson Laboratory (USA) and backcrossed for seven generations with C57BL/6J mice purchased from Charles River (France). Intercrossing of these mice with B6.Cg-Tg(S100A8-cre,-EGFP)1llw/J (MRP8-Cre-ires/GFP, RRID IMSR\_JAX:021614) obtained from the Jackson Laboratory (USA) resulted in PAD4<sup>fl/fl</sup> × MRP8Cre-ires/GFP (hence forward abbreviated as Ne-PAD4<sup>-/-</sup>). Breeding of PAD4<sup>fl/fl</sup> with Ne-PAD4<sup>-/-</sup> mice resulted in litters containing both PAD4<sup>fl/fl</sup> and Ne-PAD4<sup>-/-</sup> offspring due to the hemizyosity of the *MRP8Cre* gene.

Knockout mice (Ne-PAD4<sup>-/-</sup>), together with littermate controls (PAD4<sup>fl/fl</sup>), were aged for 24 months. Separate groups of 9- to 12-week-old mice from the same breeding colony were used as young controls. The study includes both male and female animals. Mice were kept on a standard laboratory diet (ssniff #R/M-H) for the entirety of the study. All groups were age- and sex-matched and received *ad libitum* feed, with free access to water. All animal interventions were performed during morning hours in order to take circadian rhythms of both mice and neutrophils into account. All analyses were performed by an investigator blinded to the identities of the mice. There was no randomization performed, as the breeding scheme results in expected Mendelian ratios of 50:50 *MRP8Cre*<sup>+</sup> to *MRP8Cre*<sup>-</sup> animals (as tracked in 605 mice over 2.5 years).

### (b) Echocardiography

Cardiac function and dimensions were measured via echocardiography, using a Vevo 2100 3D analyzer (Fujifilm Visualsonic). Mice were anesthetized using 2% isoflurane in medical oxygen at a flow rate of 2.5 l/min. Body temperature was constantly monitored via a rectal probe and kept between 35.5°C and 37°C. Heart rate was kept stable between 450 and 550 BPM for all measurement acquisitions. In the parasternal long axis (PLAX), cardiac dimensions were evaluated using Brightness (B)-mode. Using pulsed wave (PW) Doppler, the blood flow and pressure in the pulmonary artery were measured. In the parasternal short axis (PSAX), Motion (M)-mode was used to measure left ventricular posterior wall (LVPW) thickness, left ventricular internal diameter (LVID) and left ventricular anterior wall (LVAW) thickness. In the apical 4 chamber (A4C) window, the PW Doppler was placed at the level of mitral inflow to measure blood flow into the left ventricle (LV) coming from the left atrium. Using PW Doppler in the pulmonary artery, right ventricular pulmonary ejection time (PET) and pulmonary acceleration time (PAT) were measured. Finally, blood flow in the aorta was measured using PW Doppler. Echocardiographic recordings were stored digitally and analysed using the Vevo Lab software (Vevo lab, V.5.5.1). Left ventricular ejection fraction (LVEF) was calculated based on Simpson's method using the simplified Quinones method. Blood flow in the A4C view was used to determine signs of impaired LV relaxation, as ease of ventricular filling is expressed as the ratio between the *E* and the *A* wave (*E/A*).

### (c) Blood cell counts and plasma preparation

At time of euthanasia, mice were anesthetized using a mixture of ketamine/xylazine at a non-lethal dose ( $125 \text{ mg kg}^{-1}$  and  $12.5 \text{ mg kg}^{-1}$ , respectively). Once mice were non-responsive to pedal-reflex (toe pinch), blood was collected via the retroorbital sinus into 3.8% citrate anticoagulant in a 1/10 (vol/vol) dilution using a pre-coated capillary. An aliquot of blood was run on the automated Scil Vet ABC Plus+ (Scil) system for automated calculation of peripheral blood counts. The remaining blood was centrifuged at 3000 g for 5 min, after which the supernatant was transferred to a clean tube and centrifuged again for 5 min at 12 300 g. After centrifugation, platelet-poor plasma was transferred to a clean tube and immediately stored at  $-20^\circ\text{C}$  for future batch analysis.

### (d) Histology

Ketamine/xylazine anesthetized mice were perfused using 0.9% saline until liver paleness was verified, after which organs were removed. Hearts were fixed in 4% paraformaldehyde in phosphate-buffered saline (PBS) overnight at  $4^\circ\text{C}$ . After washing 3 times in PBS, fixed hearts were kept in 70% ethanol at  $4^\circ\text{C}$  until further processing and paraffin embedding. Tissue was sectioned in  $8 \mu\text{m}$  slices and rehydrated. To assess collagen content in heart tissue, Masson trichrome (Sigma Aldrich) and Fast Green/Sirius Red (Chondrex) staining were performed according to the manufacturers' protocols. After staining, slides were dehydrated and mounted using DPX mounting medium (Sigma Aldrich). Heart sections were then visualized at 100X magnification in bright-field microscopy in a blinded manner. Mosaic images were acquired using the MosaiX tool in Axiovision software (Zeiss). Images were used to quantify collagen content as a percentage of the total area by colour thresholding analysis in ImageJ software (FIJI) [31]. To evaluate perivascular fibrosis, three random blood vessels were selected in the LV of each section.

To determine cardiomyocyte surface area, heart sections were stained using wheat germ agglutinin (WGA)—AlexaFluor647 conjugate (Invitrogen). Heart sections were rehydrated and then incubated with the WGA for 30 min at RT ( $10 \mu\text{g ml}^{-1}$ ), after which sections were washed and counterstained using Hoechst 33342 (1/10,000) (Sigma) and mounted for microscopy. Slides were imaged using a Nikon Ti2 confocal microscope at 600X magnification. From the LV, four random fields of view were imaged and used for quantification of cardiomyocyte surface area in ImageJ.

### (e) RT-qPCR

Heart tissue was snap frozen in liquid nitrogen and subsequently stored at  $-80^\circ\text{C}$ . Later, tissue was mechanically ground and homogenized using ceramic beads. Homogenized tissue was used for total RNA extraction via an RNeasy mini kit (QIAGEN). Total RNA was used to construct cDNA using random hexamer primers. For cDNA construction, the QuantiTect Reverse Transcription kit, with gDNA removal step (QIAGEN), was used according to the manufacturer's instructions. Quantitative real-time PCR was performed using gene-specific primers (electronic supplementary material, table S1). SYBR Green Master Mix (Applied Biosystems) was used to perform qRT-PCR with a QuantStudio 3 Real Time PCR detection system. RT-qPCR data were analysed using the Livak and Schmittgen ( $2^{-\Delta\Delta\text{Ct}}$ ) method [32].

### (f) Plasma analyses for biomarker determination

Stored plasma was used for batch analysis detection of several inflammation biomarkers. Plasma levels of cell-free dsDNA were detected using the Quanti-iTPicoGreen dsDNA assay kit (ThermoFisher). Mouse IL-6 levels in plasma were initially detected using the ProQuantum Immunoassay kit for detection of mouse IL-6, according to manufacturer's instructions (ThermoFisher).

An in-house sandwich ELISA was used to detect plasma levels of H3Cit–DNA complexes as a biomarker for NETs in circulation. In short, a 96-well plate was incubated with a recombinant anti-citrullinated histone H3 (R2+8+17) antibody (ab281584– $1.25 \mu\text{g ml}^{-1}$ ) at  $4^\circ\text{C}$  overnight. The next day, the plate was washed and blocked using 1% bovine serum albumin (BSA) in PBS for 90 min at room temperature. Following blocking, the plate was washed 3 times and incubated with plasma samples diluted in assay buffer containing an anti-dsDNA monoclonal antibody, conjugated to peroxidase (from Cell Death Detection ELISA<sup>PLUS</sup>, Roche, 11774425001—diluted 1:50 (vol/vol) in the kit's provided incubation buffer). After incubation for 2 h at room temperature, the plate was washed 3 times and incubated with ready-to-use TMB substrate for a minimum of 10 min, after which the reaction was stopped using 1N hydrochloric acid and the absorbance measured at 450 with 630 nm background correction.

Plasma MPO–DNA complex levels were determined using an in-house ELISA. In short, a 96-well plate was coated using an anti-MPO antibody (ThermoFisher PA5-16672—diluted 1:1000 vol/vol) and incubated at  $4^\circ\text{C}$  overnight. The following day, the plate was washed and blocked using 3% BSA in PBS with 0.05% Tween-20. After blocking the plate was washed 4 times, after which it was incubated with the plasma samples for 90 min while shaking (200 rpm). After incubation with samples, the plates were again washed and incubated using a peroxidase-conjugated anti-DNA antibody (taken from Cell Death Detection ELISA<sup>PLUS</sup>, Roche, 11774425001–1:50 in incubation buffer) for a period of 90 min at room temperature, while shaking at 200 rpm. Next the plate was washed and signal was developed by adding TMB for a minimum of 10 min, after which the reaction was stopped by adding 1 N of hydrochloric acid. Finally, absorbance was measured at 450 nm with 630 nm background correction.

For multiplex cytokine detection, the V-PLEX Cytokine Panel 1 mouse MSD kit (Meso Scale Discovery) was run according to the manufacturer's instructions. This assay allowed for high-sensitivity detection of IL-15, IL-17A/E, IL27p28/IL-30, IL-33, IP-10, MCP1, MIP1a and MIP2. For multiplex detection of pro-inflammatory markers, V-PLEX Proinflammatory Panel 1 mouse kit (MSD) was performed according to the manufacturer's instructions. This assay allowed for the quantification of IFN- $\gamma$ , IL-1 $\beta$ , IL-2, IL-4, IL-5, IL-6, IL-10, IL12p70, KC/GRO and TNF- $\alpha$ . Data from V-PLEX Meso Scale experiments were analysed using the MSD discovery workbench software (MSD, LSR\_4\_0\_13) using standard curves included in the respective assays.

### (g) Statistical analysis

Data are represented as medians  $\pm$  interquartile ranges. Normality of the data was tested using a Shapiro–Wilk normality test. For statistical tests, a two-tailed Mann–Whitney *U* test was used to compare two groups. For comparison of more than two groups, one-way ANOVA was used when data had a normal distribution. For non-normal distributed data, the non-parametric Kruskal–Wallis test was applied to compare three or more groups. All tests were performed after exclusion of statistical outliers, according to ROUT's method ( $Q=1\%$ ). Correlation analysis was performed between the level of cardiac collagen, which is a measure for heart fibrosis, and both LVEF and *E/A* ratio, using simple linear regression. All statistical tests were performed using Graphpad Prism software (v.9.5).

## 3. Results

### (a) Age-induced ventricular dilation is lacking in the absence of neutrophil PAD4

Deletion of PAD4 was previously shown to decrease NET formation significantly, while having no effect on numbers of



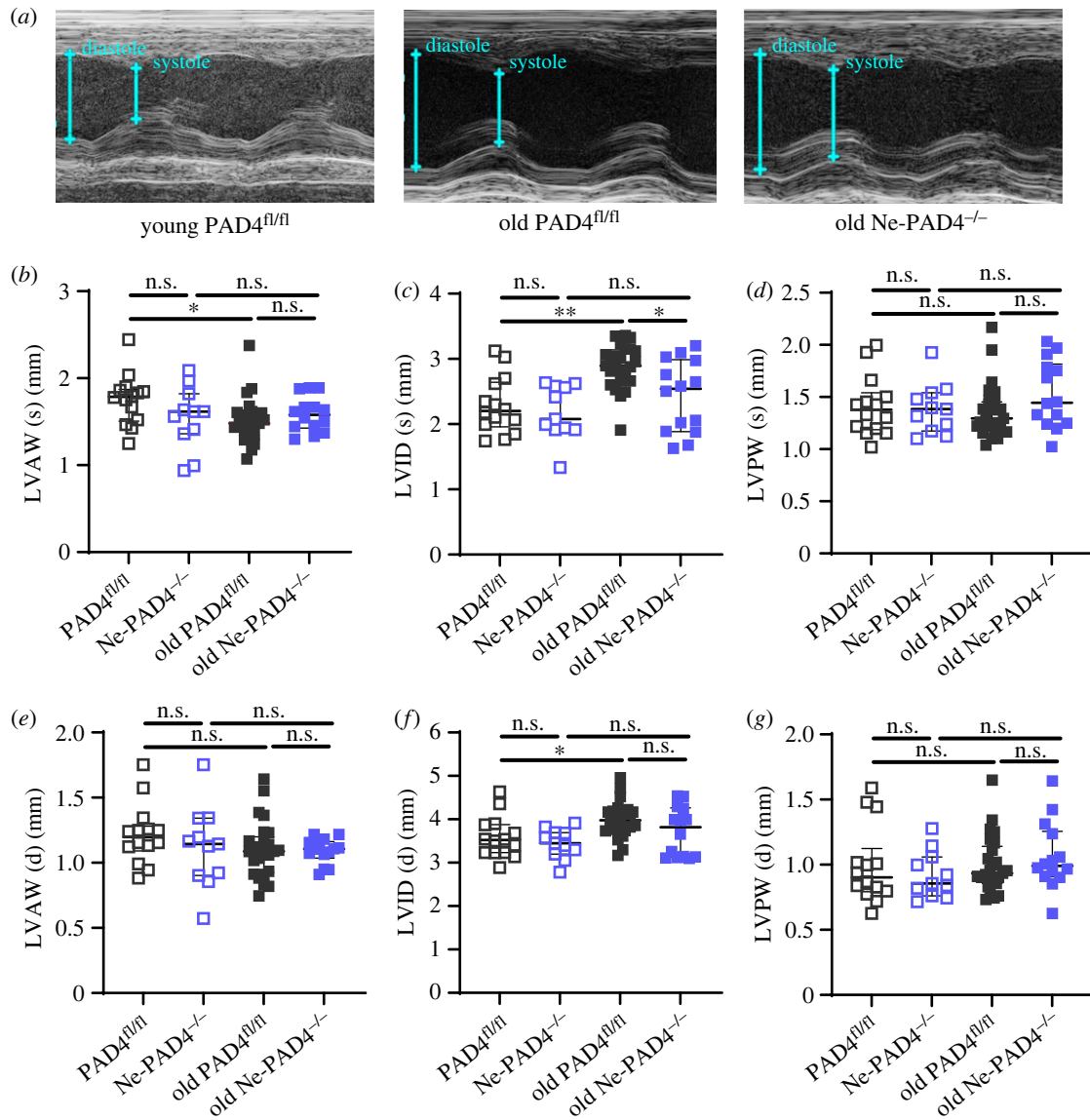


**Figure 1.** Neutrophil  $PAD4$  deletion prevents left ventricular dilation with increasing age. (a) Representative transthoracic echocardiography images of M (motion) mode recording in parasternal short axis (PSAX) window in young (9–12 weeks) and old (24 months)  $PAD4^{fl/fl}$  and  $Ne-PAD4^{-/-}$  mice. (b–d) Quantification of left ventricular dimensions of young and old  $PAD4^{fl/fl}$  and  $Ne-PAD4^{-/-}$  mice during peak systole, respectively, quantification of left ventricular anterior wall (LVAW) thickness (b), LV internal diameter (LVID) (c) and LV posterior wall (LVPW) thickness (d). (e–g) LV dimensional quantification during peak diastole, respectively for LVAW thickness (e), LVID (f) and LVPW thickness (g). n.s., not significant, \* $p < 0.05$ , \*\* $p < 0.01$ , \*\*\* $p < 0.001$ . Graphs show  $n = 10$ – $15$  for young mice, and  $n = 14$ – $25$  for old mice.

leucocytes in circulation [33,34]. In order to study the effect of neutrophil  $PAD4$  on the aged heart,  $Ne-PAD4^{-/-}$  animals were evaluated alongside littermate controls. The groups were age- and sex-matched, including both male and female mice. Using echocardiography, ventricular dimensions of both young (9–12 weeks old;  $PAD4^{fl/fl}$   $n = 15$ ,  $Ne-PAD4^{-/-}$   $n = 11$ ) and old (24 months old;  $PAD4^{fl/fl}$   $n = 25$ ,  $Ne-PAD4^{-/-}$   $n = 14$ ) mice were evaluated both at peak systole and diastole (figure 1a–g). During peak systole, no significant differences were observed in LV wall thickness, with both the LVAW (figure 1b), as well as the LVPW (figure 1d) thickness of the aged groups being comparable to young control animals. LVID (s) increased significantly in the old  $PAD4^{fl/fl}$  group in comparison to both the young control group and the  $Ne-PAD4^{-/-}$  aged group (figure 1c). During diastole, no changes in either LVAW (figure 1e) or LVPW (figure 1g) were observed between young and old groups. However, the old  $PAD4^{fl/fl}$  showed a significant dilation of the left ventricle (LVID) (d)

to the young  $PAD4^{fl/fl}$  animals (figure 1f). Interestingly, this dilation was absent in the old  $Ne-PAD4^{-/-}$ , with LVID (d) being comparable to their young controls (figure 1f).

### (b) $Ne-PAD4^{-/-}$ mice are protected against collagen deposition in the ageing heart

Ageing is one of the most predisposing factors for fibrotic heart diseases [35]. Therefore, cardiac collagen deposition was evaluated as a marker for cardiac fibrosis in young versus old  $PAD4^{fl/fl}$  and  $Ne-PAD4^{-/-}$  animals. Corrected heart weight (heart weight divided by tibia length) has previously been used as an overall measure for cardiac hypertrophy development with increasing age [36]. The corrected heart weight of  $PAD4^{fl/fl}$  mice was significantly increased with increasing age, while this increase was absent in aged  $Ne-PAD4^{-/-}$  mice (figure 2a). In addition, total collagen content in the heart was imaged and quantified using Masson's trichrome

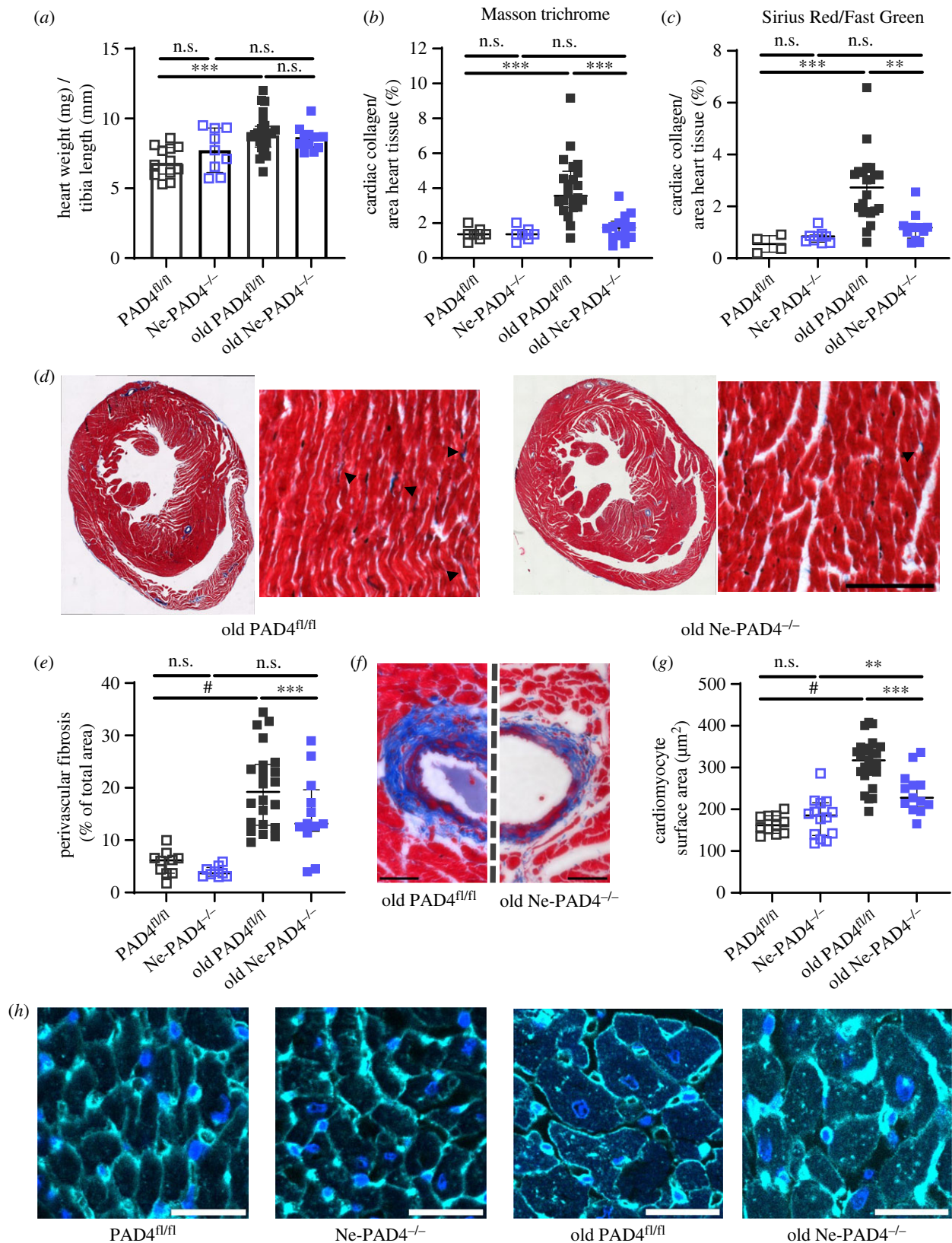


Figure 2. (Caption overlaid.)

(figure 2*b,d*), and Fast Green/Sirius Red staining (figure 2*c*). Aged *PAD4*<sup>fl/fl</sup> mice had significantly more cardiac collagen deposition as compared to age-matched *Ne-PAD4*<sup>-/-</sup> mice (figure 2*b,c*). At nine weeks of age, collagen content in the heart muscle was comparable between both genotypes indicating that the observed increase in collagen content in the old *PAD4*<sup>fl/fl</sup> mice can indeed be classified as an age-related event. Of equal interest, in old *Ne-PAD4*<sup>-/-</sup> mice the

amount of fibrotic tissue remains similar to that of young *Ne-PAD4*<sup>-/-</sup> mice as observed by both Masson trichrome staining and Fast Green/Sirius Red staining. In addition to overall cardiac collagen, perivascular fibrosis, as quantified by collagen area surrounding cardiac blood vessels, significantly increased with increasing age in *PAD4*<sup>fl/fl</sup> mice but not in *Ne-PAD4*<sup>-/-</sup> mice (figure 2*e,f*). Here we observed that perivascular fibrosis of old *PAD4*<sup>fl/fl</sup> mice was also

**Figure 2.** (*Overleaf.*) PAD4 deficiency in neutrophils specifically reduces cardiac hypertrophy and collagen deposition with increasing age. (a) Heart weight of mice was corrected for animal size by dividing by tibia length. Increase in corrected heart weight was taken as a measure for increased cardiac remodelling. (b,c) Cardiac collagen content was assessed by both Masson trichrome and Fast Green/Sirius Red stain in both young and old PAD4<sup>fl/fl</sup> and Ne-PAD4<sup>-/-</sup> mice. Total collagen was quantified as the percentage of collagen in the whole heart section. (b) The percentage of fibrotic area (blue fibres) in the heart tissue of Masson trichrome-stained section was quantified through the colour threshold application in ImageJ. Equal colour thresholding settings were applied for both young and old mice. (c) Quantification of collagen (Bordeaux fibres) of Fast Green/Sirius Red-stained heart tissue of young and old PAD4<sup>fl/fl</sup> and Ne-PAD4<sup>-/-</sup> mice. Quantification was done through colour thresholding on ImageJ. (d) Representative images of Masson trichrome staining of a horizontal cross-sectional area of mouse heart of old PAD4<sup>fl/fl</sup> and Ne-PAD4<sup>-/-</sup> mice. Cardiomyocytes are stained red, collagen fibres are stained blue. Beside whole heart sections, representative images at 200X magnification of Masson trichrome-stained LV wall are shown. Arrowheads indicate the presence of interstitial collagen fibres in the heart tissue. Scale bar: 100  $\mu$ m. (e) Perivascular fibrosis, quantified as the amount of collagen deposition around the blood vessel through colour thresholding using ImageJ. (f) Representative presentation of cardiac blood vessels in the left ventricle of old PAD4<sup>fl/fl</sup> and old Ne-PAD4<sup>-/-</sup> mice. (g) Quantification of cardiomyocyte hypertrophy through cell surface area in the left ventricle of the mouse heart. Cell surface area was calculated through manual lining of the cells of the LV using ImageJ. (h) Representative images of wheat germ agglutinin (WGA)-staining of the left ventricle of young and old PAD4<sup>fl/fl</sup> and Ne-PAD4<sup>-/-</sup> hearts. WGA staining was adopted to line cell membrane, which enabled cellular delineation and cell surface calculation. Scale bar represents 25  $\mu$ m. n.s., not significant, \* $p < 0.05$ , \*\* $p < 0.01$ , \*\*\* $p < 0.001$ ; #,  $p < 0.0001$ . Graphs show  $n = 10$ – $15$  for young mice, and  $n = 14$ – $25$  for old mice.

significantly elevated as compared to Ne-PAD4<sup>fl/fl</sup> mice. In addition to fibrotic remodelling, cardiomyocyte hypertrophy was assessed through quantitative measurement of cardiomyocyte surface area. Increasing age resulted in an expansion of cardiomyocyte cell surface area in both PAD4<sup>fl/fl</sup> and Ne-PAD4<sup>-/-</sup> mice. However, cardiomyocyte surface area of PAD4<sup>fl/fl</sup> was significantly enhanced with increasing age as compared to Ne-PAD4<sup>-/-</sup> cardiomyocytes at similar age (figure 2g,h).

### (c) Age-induced decline in heart function is absent in Ne-PAD4<sup>-/-</sup> mice

By contrast to humans, mice have progressively declining systolic function with age. In our study set, increasing age was associated with a decrease in cardiac systolic function in PAD4<sup>fl/fl</sup>, but not Ne-PAD4<sup>-/-</sup> mice. Left ventricular contraction was clearly impaired for PAD4<sup>fl/fl</sup> mice, as seen by an increased residual volume inside the ventricle during peak systole (figure 3a). Deletion of PAD4 under the MRP8 promoter did not result in a reduction in systolic function itself at young age, as evaluated by left ventricular fractional shortening (FS) (figure 3b), and LVEF (figure 3c). However, at 24 months FS and LVEF of PAD4<sup>fl/fl</sup> mice significantly decreased as compared to young controls as well as old Ne-PAD4<sup>-/-</sup> mice (figure 3b,c). The observed LVEF values in 24-month-old PAD4<sup>fl/fl</sup> are consistent with previously published results for wild-type animals of a similar age [20]. Our data show that LVEF in the PAD4<sup>fl/fl</sup> genotype dropped from  $67 \pm 2\%$  in the young group to  $53 \pm 2\%$  in the old PAD4<sup>fl/fl</sup> group. By contrast, LVEF in the old Ne-PAD4<sup>-/-</sup> group remained constant over the 2-year period (young— $66 \pm 2\%$ , old— $67 \pm 2\%$ ) (figure 3b). This result is in agreement with the systemic PAD4<sup>-/-</sup> mice we have previously described [20].

Considering the effect that ageing has on diastolic function in humans, we also investigated this in our mice. Atrial to ventricular filling was measured to assess diastolic function of the LV. Specifically, the mitral inflow pattern was measured, and the ratio between the *E* wave (representing early, passive filling of the LV due to opening of the mitral valve) and the *A* wave (representing late active filling due to atrial contraction) was calculated. In the old PAD4<sup>fl/fl</sup> mice, the mean *E/A* ratio significantly decreased compared to young PAD4<sup>fl/fl</sup> mice (figure 3d,e). Of note, this evolution

towards diastolic dysfunction was absent in the old Ne-PAD4<sup>-/-</sup> mice (figure 3d,e). Additionally, the isovolumetric relaxation time (IVRT), which is defined as the time between aortic ejection and ventricular filling, was used to evaluate ventricular compliance and relaxation. For PAD4<sup>fl/fl</sup> mice, IVRT significantly increased in old age as compared to young controls (figure 3f). In Ne-PAD4<sup>-/-</sup> mice, however, IVRT remained constant over the 2-year period (figure 3f). In young mice, diastolic function, both defined by the *E/A* ratio and the IVRT, did not differ across the two genotypes. Overall, cardiac function between the four experimental groups can be visualized through a radar plot, from which it is clear that both cardiac function and structure of old PAD4<sup>fl/fl</sup> deviate from the three other experimental groups (figure 3g).

In order to evaluate whether this observed difference in fibrosis between both genotypes at old age was associated with differences in cardiac function, myocardial fibrosis levels, as determined by Masson trichrome staining, were correlated with both systolic function (via LVEF; figure 3h) as well as diastolic function (via *E/A*; figure 3i). Correlation analysis of cardiac fibrosis level with LVEF, showed a significant ( $p = 0.003$ ) negative correlation with a Spearman correlation coefficient ( $r$ ) of  $-0.41$ . In addition, correlation analysis of fibrosis level with diastolic function through *E/A* ratio revealed a significant ( $p = 0.016$ ) negative correlation with  $r = -0.35$ . From this we can conclude that neutrophil *Padi4* plays a crucial role in the deterioration of cardiac function with increasing age, and that this correlates with fibrotic remodelling.

### (d) Chemotactic gene expression is reduced in old Ne-PAD4<sup>-/-</sup> mice hearts

It is widely known that ageing coincides with a number of physiological changes. Gene expression is altered with increasing age, possibly explaining declines in both physical and cognitive abilities [37]. Since we were mainly interested in cardiac ageing, and investigating the complex interplay between neutrophil *Padi4*, age and cardiac dysfunction, with a particular interest in cardiac fibrosis as an underlying mechanism, we examined gene expression in heart tissue. Hearts were perfused and harvested from PAD4<sup>fl/fl</sup> ( $n = 13$ ) and Ne-PAD4<sup>-/-</sup> ( $n = 9$ ) mice at 24 months, after which total RNA was isolated and used to perform quantitative real-time PCR to compare



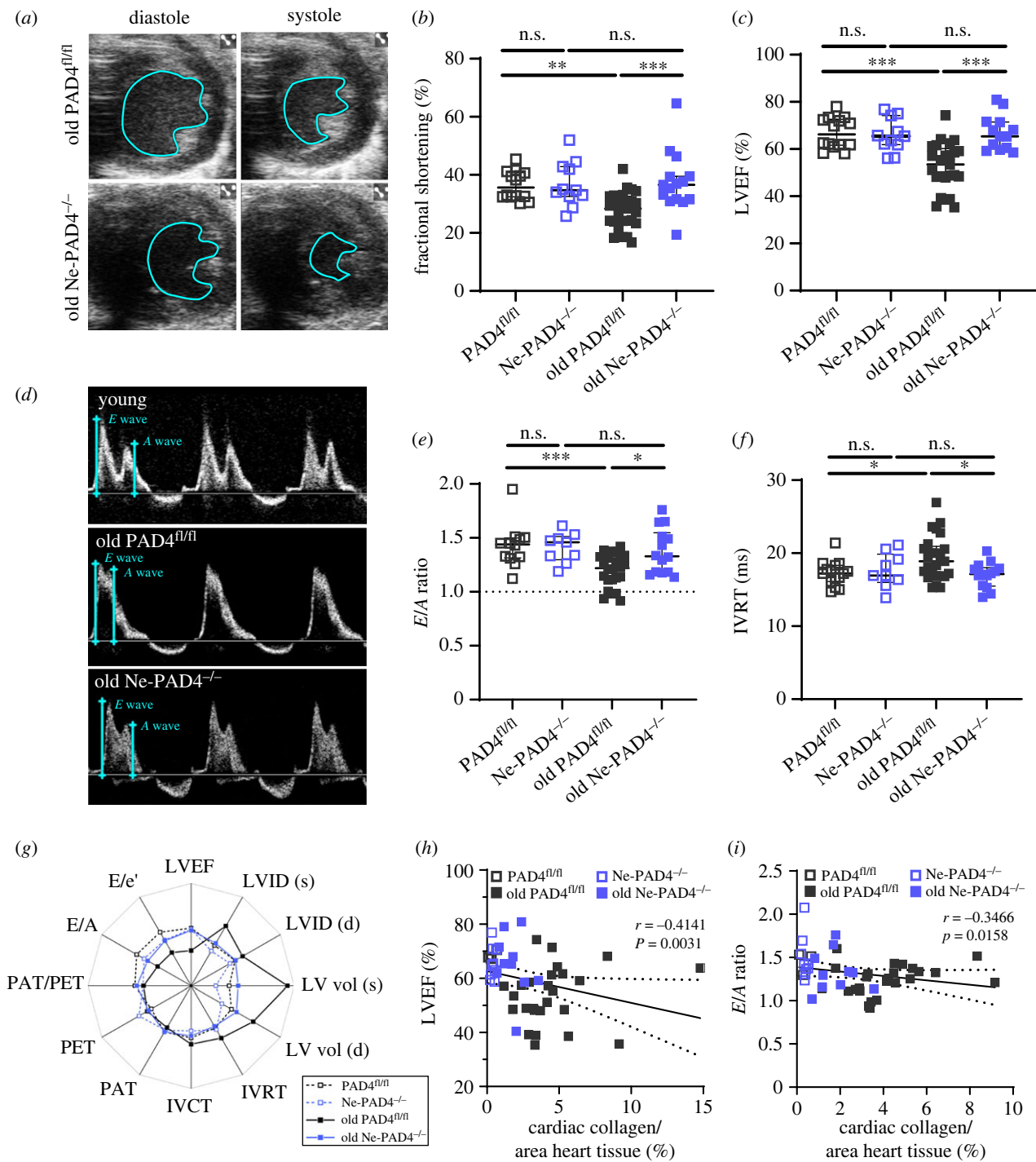


**Figure 3.** Ne-PAD4<sup>-/-</sup> mice maintain cardiac function comparable to young mice. (a) Representative PSAX transthoracic echocardiography images of the left ventricle at peak diastole and systole of both old (24 months) PAD4<sup>fl/fl</sup> and old Ne-PAD4<sup>-/-</sup> mice. (b) Quantification of left ventricular systolic function through fractional shortening (FS) of the left ventricle. (c) Quantification of left ventricular ejection fraction (LVEF) based on a simplified Quinone's method, calculated through end systolic and end diastolic volumes. (d) Representative pulsed wave (PW) Doppler echocardiography images in the apical 4 chamber (A4C) window. Ventricular diastolic function was evaluated in young and old PAD4<sup>fl/fl</sup> and Ne-PAD4<sup>-/-</sup> mice through the flow pattern across the mitral valve. (e,f) LV ventricular diastolic function was evaluated through the filling pattern, evaluated and calculated as the ratio between the E and A waves and the isovolumetric relaxation time (IVRT) as the time between aortic ejection and early LV filling. (e) Calculation and quantification of LV filling pattern by taking the E/A ratio. A E/A ratio equal to 1.5 ( $E > A$ ) is taken as a normal pattern, while  $E < A$  is a reversed pattern. (f) Quantification of IVRT in young and old PAD4<sup>fl/fl</sup> and Ne-PAD4<sup>-/-</sup> mice; increasing IVRT is evidence of impaired LV filling. (g) Radar plot of general cardiac function and dimensions of both young and old PAD4<sup>fl/fl</sup> and Ne-PAD4<sup>-/-</sup> mice. IVCT, isovolumetric contraction time. (h,i) Correlation analysis, including all the experimental groups, between the percentage of fibrosis, as determined by the Masson trichrome staining, and systolic cardiac function, given by LVEF (h) or diastolic function, given by E/A ratio (i). n.s., not significant, \* $p < 0.05$ , \*\* $p < 0.01$ , \*\*\* $p < 0.001$ . Graphs show  $n = 9$ –12 for young mice, and  $n = 14$ –25 for old mice.

gene expression levels in the aged heart tissue. We selected genes involved in fibrosis (*Agt*, *Ccl12*, *Ccn2*, *Tgfb*, *Col1a3*, *Col3a1*, *Mmp3*, *Mmp9*, *Mmp13*, *Timp1*, *Timp2*, *Timp3*, *Timp4*), inflammation (*Ccl3*, *Ifng*, *Il10*, *Tnf*, *Smad3*, *Smad4*) and general

heart failure (HF) markers (*Nppa*, *Nppb*) for evaluation of expression levels. In the hearts of the old Ne-PAD4<sup>-/-</sup> mice, collagen type III, alpha-1 (*Col3a1*) and tissue inhibitor of metalloprotease 3 (*Timp3*) were upregulated (figure 4—red bars),

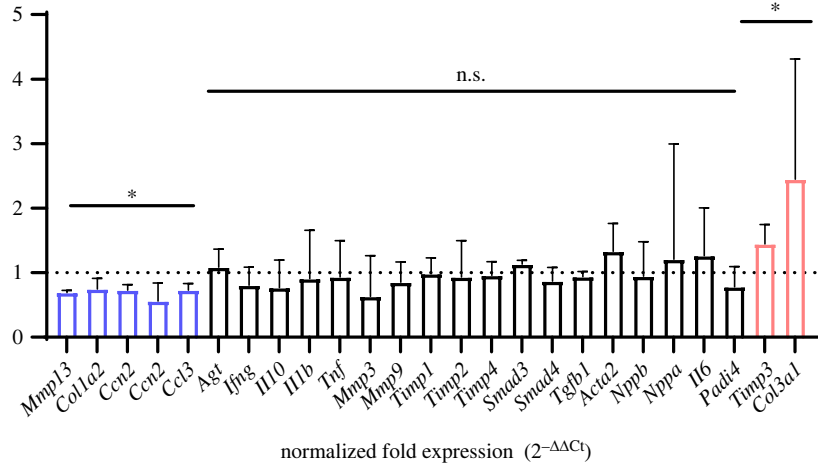


**Figure 4.** Gene expression in the ageing heart is altered due to PAD4 deletion in circulating neutrophils. Quantitative real-time RT-PCR analysis was performed for mRNA expression of several genes in heart tissue from old Ne-PAD4<sup>-/-</sup> mice. Fold expression was calculated with glyceraldehyde 3-phosphate dehydrogenase (GAPDH) as a reference gene, and normalized to mRNA expression in old PAD4<sup>fl/fl</sup> hearts. Changes in gene expression (up- or downregulated) were taken to be significant when normalized fold expression ( $2^{-\Delta\Delta C_t}$ ) significantly differed from a mean of 1. n.s., not significant, \*  $p < 0.05$  by Wilcoxon signed-rank test with hypothetical value set to one. For old PAD4<sup>fl/fl</sup> and Ne-PAD4<sup>-/-</sup> groups,  $n = 9-13$ .

while C-C motif chemokine 3 (*Ccl3*), C-C motif chemokine 12 (*Ccl12*), CCN family member 2 (*Ccn2*), matrix metalloproteinase 13 (*Mmp13*) and collagen 1 alpha-3 (*Col1a2*) were downregulated as compared to the old PAD4<sup>fl/fl</sup> mice (figure 4—blue bars). The remaining genes did not significantly differ in expression levels (figure 4—black bars). This indicates a modest profile of protective gene expression changes related to collagen deposition and, notably, leucocyte recruitment.

### (e) Plasma levels of chemotactic cytokines are reduced in old Ne-PAD4<sup>-/-</sup> mice

As the gene expression changes in heart tissue were modest, we next investigated the impact of neutrophil PAD4 deficiency on the systemic circulation. Blood composition analysis of young and old mice of both genotypes revealed a marked alteration in composition accompanied by natural ageing. Levels of circulating platelets increased significantly in both genotypes with increasing age (figure 5*a*), while white blood cell numbers decreased in both aged groups compared to their young controls (figure 5*b*). This drop in total white blood cells can be attributed to a clear decrease in lymphocytes with increasing age, as granulocyte, monocyte and eosinophil cell numbers are comparable between both young and old ages, as well as across genotypes (electronic supplementary material, figure S1). The neutrophil-to-lymphocyte ratio, often indicating ongoing inflammation, was calculated. This was increased in old PAD4<sup>fl/fl</sup> mice compared to young controls, an observation that was absent in the old Ne-PAD4<sup>-/-</sup> group compared to their young counterparts (figure 5*c*). Subsequently, plasma biomarkers for both ageing and inflammation were quantified for both genotypes, both at young and old ages. As a general marker of ageing, cell-free dsDNA (cfDNA) was evaluated [38]. An increase in levels of cfDNA was observed in both old PAD4<sup>fl/fl</sup> and Ne-PAD4<sup>-/-</sup> mice as compared to their young controls (figure 5*d*). Following this observation, plasma levels of citrullinated histone H3 (H3Cit)-DNA complexes (figure 5*e*) as well as MPO-DNA complexes

(figure 5*f*) were determined as more specific biomarkers for NETs in circulation. However, no significant difference in both markers could be observed between both genotypes and across the different age categories. Next, plasma levels of circulating cytokines (IL-15, IL-17A, IL27 $\alpha$ , IL-33, CXCL10, CCL2, CCL3 and CXCL2), as well as pro-inflammatory markers (IFN- $\gamma$ , IL-1 $\beta$ , IL-2, IL-4, IL-5, IL-6, IL-10, IL-12, CXCL1 and TNF- $\alpha$ ) were evaluated and compared between genotypes and age groups (figure 5*g,h*). Overall, an increase could be seen in circulating cytokines in the old PAD4<sup>fl/fl</sup> genotype as compared to both young controls and the old Ne-PAD4<sup>-/-</sup> group (figure 5*g*). Additionally, an age-related decrease in certain inflammatory cytokines (IFN- $\gamma$ , IL-10, IL-1 $\beta$ , IL-12, IL-2 and IL-4) could be observed in both genotypes, while others (IL-6, CXCL1 and TNF- $\alpha$ ) demonstrated an age-related increase in plasma levels in the old PAD4<sup>fl/fl</sup>, but not in the old Ne-PAD4<sup>-/-</sup> genotype (figure 5*h*). Plasma levels of pro-inflammatory interleukin 6 (IL-6) were significantly upregulated in the old PAD4<sup>fl/fl</sup> as compared to the old Ne-PAD4<sup>-/-</sup> mice (figure 5*i*). As compared to young controls, the plasma levels of tumour necrosis factor  $\alpha$  (TNF $\alpha$ ) were significantly upregulated in the PAD4<sup>fl/fl</sup> mice, while this increase was absent in the Ne-PAD4<sup>-/-</sup> genotype (figure 5*j*). Both C-C ligand 2 (CCL2) and C-C ligand 3 (CCL3) plasma levels were significantly increased in old mice, as compared to their young controls for both genotypes (electronic supplementary material, figure S2*A,B*). However, members of the C-X-C motif family behaved differently. A significant increase could be measured in the protein concentration of C-X-C ligand 1 (CXCL1) in the plasma of old PAD4<sup>fl/fl</sup> as compared to young controls, while this increase in plasma levels was absent in old mice with the Ne-PAD4<sup>-/-</sup> genotype (figure 5*k*). Furthermore, a significant difference could be seen between plasma levels of CXCL1 between the two aged groups. Additionally, plasma levels of C-X-C motif ligand 2 (CXCL2) were studied, as this chemokine is important in the recruitment of polymorphonuclear leucocytes, and a known therapeutic target in CVD. However, plasma levels of CXCL2 in old PAD4<sup>fl/fl</sup> mice were not significantly increased compared to young controls ( $p = 0.07$ ),



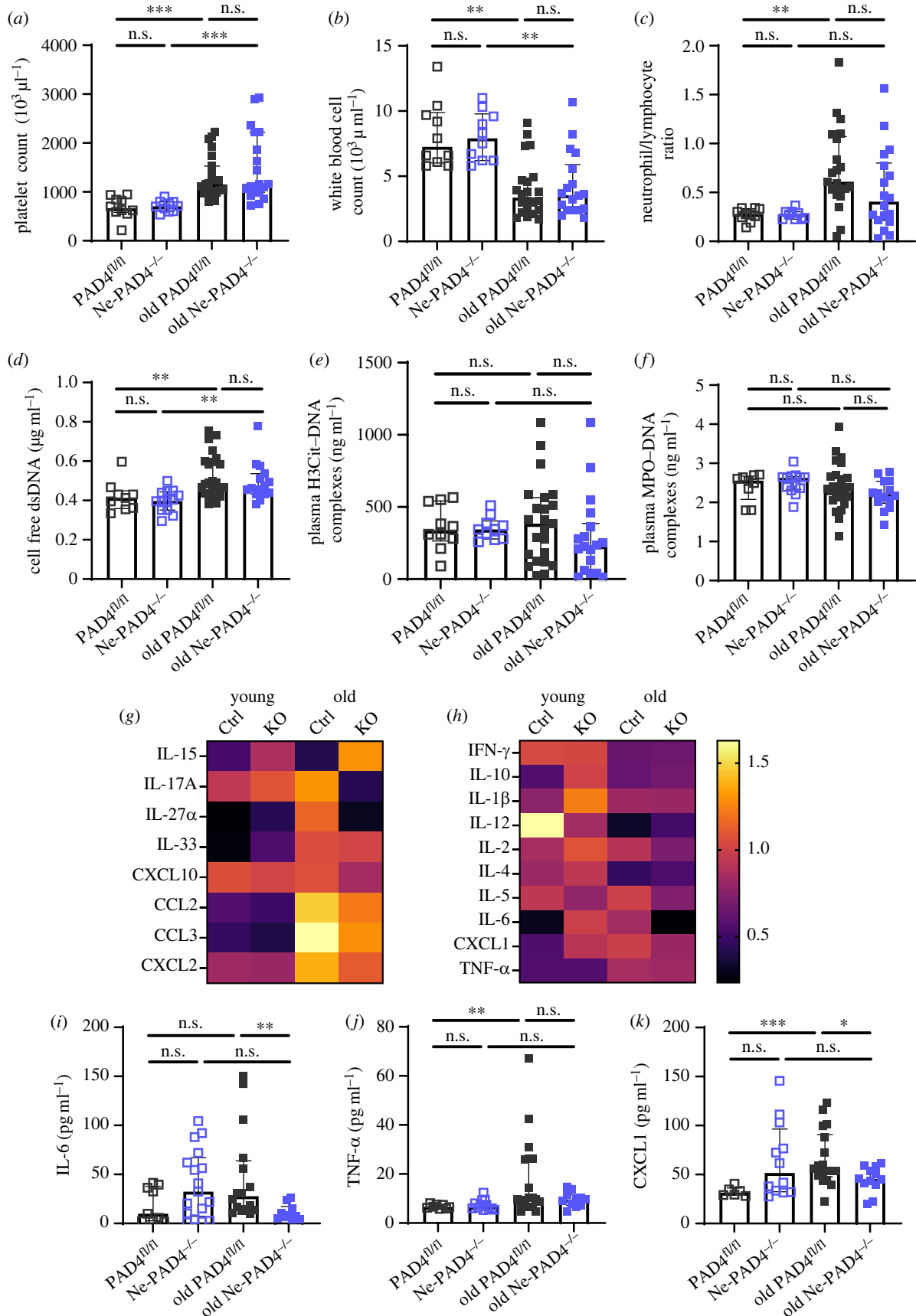


**Figure 5.** Old Ne-PAD4<sup>-/-</sup> mice have a decreased pro-inflammatory status with a reduced chemotaxis profile. (a–c) Peripheral blood counts, determined at young and old ages. (a) Peripheral platelets and (b) white blood cells. (c) Calculation of the neutrophil–lymphocyte ratio as a general marker for inflammation. (d) Plasma levels of cfDNA. (e–f) Levels of circulating H3Cit–DNA complexes (e) and MPO–DNA complexes (f) in the plasma at the day of sacrifice. (g,h) Heat maps showing relative plasma levels of circulating cytokines and chemokines in the different groups of mice. Rows are corrected by dividing by the average of the row. Black, red and yellow colours indicate increased, equal and decreased plasma levels of the molecule, respectively, as compared to the average over the two genotypes and two age groups. (i) Quantification of circulating levels of IL-6. (j) TNF- $\alpha$  concentration as measured in plasma samples. (k) Plasma levels of the neutrophil chemotactic C-X-C Ligand 1 (CXCL1). n.s., not significant, \* $p < 0.05$ , \*\* $p < 0.01$ , \*\*\* $p < 0.001$ . For young groups  $n = 10$ – $17$ ; for old groups  $n = 14$ – $19$ .

nor did they differ from old Ne-PAD4<sup>-/-</sup> mice (electronic supplementary material, figure S2C).

## 4. Discussion

Increasing age, particularly over the age of 65, is the highest risk factor for the development of cardiovascular disease and HF in humans. Moreover, HF is the leading cause of death in the aged population [5]. Considering the recent projections of the World Health Organization stating that the global population over the age of 60 will increase up to 1.4 billion by 2050, it is clear that HF will grow as a major public health burden in the future. In order to mitigate this, novel strategies for HF prevention and healthy cardiac ageing are needed. We previously showed that systemic deletion of PAD4 resulted in reduced cardiac remodelling and dysfunction at old age [20]. In this current study, we highlight the importance of neutrophils, and more specifically PAD4 expression in neutrophils, as players that interfere with the process of healthy cardiac ageing. For this, a mouse model of deletion of *Padi4* through MRP8 (S100A8)-specific expression of the *Cre* recombinase was adopted. S100A8 expression has been reported in other cell types, including myeloid progenitor cells in the bone marrow. Indeed, analysis of 10X genomics RNA sequencing of mice bone marrow (open access data—Cell × Gene, Tabula Muris Senis; see <https://tabula-muris-senis.ds.czbiohub.org>) reveals activity of the promoter in granulocyte and macrophage progenitor cells in addition to neutrophils (electronic supplementary material, figure S3A,B). However, further analysis reveals the absence of *Padi4* expression by this specific subpopulation of bone marrow-derived cells (electronic supplementary material, figure S3A,C). Therefore, activity of the MRP8 promoter and subsequent deletion of *Padi4* is unlikely to affect downstream pathways in these cell types. Therefore, the use of our mouse model to investigate the long-term effects of neutrophil-derived PAD4 is unlikely to be affected by MRP8 expression in other cell types. Confirmation of these results in a secondary neutrophil-specific *Cre*-expressing mouse strain such as Ly6G-*Cre* would be of value in a future study.

Here, we observed an increase in LVID with increasing age in PAD4<sup>fl/fl</sup> mice. However, this structural change in the LV was not present in old Ne-PAD4<sup>-/-</sup> mice, with LV internal diameters being comparable to young healthy controls during both peak systole and diastole. In addition, cardiac function of old mice was evaluated for both changes in systolic and diastolic function of the LV, as well as changes in right ventricle (RV) afterload. As expected, PAD4<sup>fl/fl</sup> animals showed an age-dependent decline in heart function comparable to values previously described in wild-type mice [20]. However, parameters for both systolic function (FS, LVEF), as well as diastolic function (*E/A*, and IVRT) in old Ne-PAD4<sup>-/-</sup> mice did not show signs of age-induced deterioration and malfunction. This decrease in function deterioration in Ne-PAD4<sup>-/-</sup> mice is consistent with the previously established phenotype in systemic PAD4<sup>-/-</sup> mice [20], indicating that the phenotype is neutrophil-driven.

Previous experimental as well as clinical studies have already provided extensive evidence suggesting that the ageing heart undergoes aberrant fibrotic remodelling [39]. During this process collagen content in the heart increases, leading to progressive stiffening of the ventricles and impaired diastolic function. Cardiac collagen content was assessed as a

measure for cardiac fibrosis in both young and old mice. PAD4<sup>fl/fl</sup> showed an age-dependent increase in cardiac collagen content, which is consistent with previous descriptions in other reports [20,39]. Strikingly, in our setting of MRP8-specific deletion of *Padi4* we could observe a cardiac collagen content that did not differ between young and old groups.

Next, because of the protection against age-induced cardiac collagen deposition in the Ne-PAD4<sup>-/-</sup> mice, downstream pathways impacted by neutrophil PAD4 and how they could be involved in collagen deposition in the heart were studied. Fibrotic remodelling is known to be a complex multi-stage process, in which bone marrow-derived leucocytes are crucial [10]. When comparing hearts of both genotypes at old age, changes in cardiac gene expression could be observed as a result of neutrophil *Padi4* deletion. The simultaneous upregulation of *Col3a1* and downregulation of *Col1a2* seem contradictory; however, these two types of collagen have distinct molecular makeup and functional properties. Type I collagen fibrils are the most abundant, and are stiff structures, rendering tissue rigid and durable [40,41]. On the other hand, type III collagen fibrils are thinner than type I, and are present in high concentrations in tissues that require elastic properties [42]. *Timp3*, upregulated in Ne-PAD4<sup>-/-</sup> mice, has been shown to be both involved in cardiac fibrosis clearance, as well as in amelioration of inflammation, with TIMP3<sup>-/-</sup> mice showing both increased cardiac collagen content and a significant increase of cardiac-infiltrated neutrophils in a model of angiotensin II-induced cardiac hypertrophy [43]. Additionally, high expression levels of *Timp3* result in protection of cardiomyocytes against apoptosis in acute injury settings [44], while TIMP3 deficiency leads to dilated cardiomyopathy in mice [45]. On the other hand, *Mmp13* is downregulated in the hearts of Ne-PAD4<sup>-/-</sup> mice as compared to PAD4<sup>fl/fl</sup>. MMP13 is involved in ECM degradation, including triple helical collagens containing types I, II and III, and is shown to be upregulated in hypertensive hearts of rats [46]. Clinically, MMP13 is targeted by doxycycline administration in patients suffering from HF [47]. In accordance, it was shown that inhibition of MMP13 in a model of LV pressure overload in mice reduced cardiac hypertrophy and resulted in protection against hypertension-induced cardiac dysfunction, suggesting that MMP13 plays a detrimental role in pressure overload-induced HF [48].

In addition, several pro-inflammatory genes were downregulated in old Ne-PAD4<sup>-/-</sup> mice as compared to the old PAD4<sup>fl/fl</sup>. The C–C motif ligand 3 (*Ccl3*) was demonstrated to have a reduced expression level in the old Ne-PAD4<sup>-/-</sup> mice, as compared to old PAD4<sup>fl/fl</sup> controls. This C–C motif chemokine is known to be upregulated in HF patients [49] and it causes intracellular calcium release and recruitment of neutrophils [50], thus having a possible role in NET formation and cardiac inflammation, respectively. Interestingly, *Ccl12* was downregulated in the neutrophil PAD4 knockout group. This chemotactic factor attracts eosinophils, monocytes and lymphocytes to sites of inflammation. In addition, it has been shown that this chemokine is responsible for fibrocyte recruitment towards the lung tissue under acute injury settings, orchestrating a fibrotic response at the site of injury [51]. Finally, a potential interaction between neutrophil *Padi4* and CCN family member 2 (*Ccn2*) was uncovered. This CCN2 family member 2 promotes fibrosis development, and is involved in the ageing process. From recent research, it has been elucidated that

CCN2 is an autocrine regulator of fibroblast activation, modulating fibrosis development in the heart [52]. Interestingly, in Ne-PAD4<sup>-/-</sup> mice, *Ccn2* is downregulated at old age, as compared to age-matched PAD4<sup>fl/fl</sup> mice.

Generally, increasing age impacts the composition of the circulating blood and the working mechanisms of the immune system. Here we could observe an age-dependent increase in platelet counts, while overall white blood cell numbers decreased with increasing age in both genotypes. A decrease in circulating lymphocytes is the major underlying factor responsible for the observed drop in white blood cells. A decline in the production of naive lymphocytes by the bone marrow and thymus is primarily responsible for this decline in adaptive immune function [53]. In old PAD4<sup>fl/fl</sup> mice, this decline in adaptive immune function is accompanied by an increased inflammatory status, as can be observed by an elevated neutrophil–lymphocyte ratio, something that is absent in old Ne-PAD4<sup>-/-</sup> mice. In addition, ageing is accompanied by an increase in apoptosis, and loss of both cell and tissue integrity. This could be observed by an increase in circulating cell-free dsDNA in both genotypes at old age. These increased levels of dsDNA can, therefore, be attributed to other processes than just NET formation, which would only explain a small portion of the level of dsDNA in circulation, and is something that was confirmed by determining the plasma levels of both H3Cit–DNA as well as MPO–DNA complexes, both markers of NET formation and release in circulation. Quantification of both biomarkers showed no significant increase in either of the two, suggesting no increased levels of NET release. However, the chronic characteristic together with the short lifespan of both neutrophils and NETs has to be taken into consideration when evaluating these results. As the detection of NET biomarkers was performed at the end stage of our model, we can only conclude that at 2 years of age, there are no more NETs in circulation as compared to young and healthy controls, although a clear trend towards increased NET release can be appreciated. However, this does not rule out any potential transient increases that may have occurred throughout the 2 years of natural ageing. In addition, ageing is associated with an elevated inflammatory activity, a phenomenon termed ‘inflammaging’. This was confirmed in our model by detection of increased levels of plasma TNF- $\alpha$  in old PAD4<sup>fl/fl</sup> mice as compared to young controls. Interestingly, this pro-inflammatory environment was reduced in old Ne-PAD4<sup>-/-</sup> mice. Additionally, a difference could be observed between plasma levels of IL-6 when comparing both genotypes at old age, with PAD4<sup>fl/fl</sup> mice showing increased levels as compared to Ne-PAD4<sup>-/-</sup> mice. Apart from their clear roles in inflammation and fibrosis, both TNF- $\alpha$  and IL-6 have been described as mediators of HF progression. TNF- $\alpha$  has been shown to be a mediator of myocardial dysfunction leading to HF progression [54], while IL-6 was elevated in a cohort study of HF patients, where it was associated with reduced LVEF and poorer clinical outcomes [55].

In addition to increases in inflammation status in old PAD4<sup>fl/fl</sup> mice, our study revealed that deletion of neutrophil *Padi4* prevents age-induced increase in plasma CXCL1 levels. CXCL1 is also known as neutrophil activating protein 3, and a mouse homologue of IL-8 in humans [56]. It is, therefore, a pro-inflammatory factor and is mainly involved in neutrophil chemotaxis [57]. Moreover, the CXCL1–CXCR2 axis is involved in neutrophil degranulation and NET release

[57,58]. Recent investigations demonstrated that disruption of this signalling axis has the possibility to attenuate cardiac fibrosis, hypertrophy and dysfunction in hypertensive rat hearts [59]. Altogether, neutrophil PAD4 can be proposed to play a role in neutrophil-dependent leucocyte recruitment and fibrosis in the heart muscle at old age.

In summary, understanding the mechanisms involved in age-induced organ remodelling and dysfunction is essential for developing proper treatment and care for the elderly population. Our study has shown that neutrophil PAD4 is an important factor hampering healthy cardiac ageing. This makes neutrophil PAD4 a valid therapeutic target for both HF prevention and progression treatments during settings of chronic inflammation, as is often the case during natural ageing.

## 5. Conclusion

The absence of MRP8-driven peptidylarginine deiminase 4 (*Padi4*) expression during the process of natural ageing results in healthy cardiac function at old age in mice. This lack of function deterioration can be explained in part by reduced cardiac fibrosis, with reduction in recruitment of inflammatory cells to the myocardium and in overall inflammation status due to the absence of *Padi4* in neutrophils. Further investigation into this process of immune cell recruitment to the heart vasculature and tissue may reveal novel therapeutic strategies to target PAD4 in circulation, which could prevent irreversible scarring of the heart muscle and thus HF development and progression.

**Ethics.** All experimental procedures were reviewed and approved by the Ethical Committee of the Laboratory Animal Center at the KU Leuven (Project number P019/2020), according to the Belgian Law and the guidelines from Directive 2010/63/EU of the European Parliament.

**Data accessibility.** Raw data have been deposited in the KU Leuven Data Repository: <https://doi.org/10.48804/HCSSE> [60]. The full data for echocardiography measurements are available in electronic supplementary material, table S2 [61].

**Authors' contributions.** S.V.B.: conceptualization, data curation, formal analysis, investigation, writing—original draft; S.K.: formal analysis, investigation, writing—review and editing; J.V.W.: formal analysis, investigation, methodology, writing—review and editing; K.B.: investigation, methodology, writing—review and editing; M.S.: data curation, investigation, methodology; P.C.: data curation, formal analysis, investigation, methodology; L.F.: data curation, investigation, project administration; A.V.D.B.: conceptualization, funding acquisition, investigation, resources, supervision, writing—review and editing; T.W.: conceptualization, funding acquisition, methodology, resources, supervision, writing—review and editing; K.M.: conceptualization, project administration, resources, supervision, writing—original draft, writing—review and editing.

All authors gave final approval for publication and agreed to be held accountable for the work performed therein.

**Conflict of interest declaration.** T.W. and K.M. are inventors on patent application US11400139B2 (granted, licensed). K.M. has received consulting fees from Peel Therapeutics, Inc. The other authors have nothing to disclose.

**Funding.** This work was supported by grants from the Fonds Wetenschappelijk Onderzoek Vlaanderen (grant no. G097821N to A.V.D.B. and K.M.) and (grant no. ERA-CVD JTC2019) consortium grant to A.V.D.B., T.W. and K.M. (grant no. FIBRONETx, G0G1719N).

**Acknowledgements.** We would like to thank the members of the Martiod group in the Center for Molecular and Vascular Biology, Department of Cardiovascular Science, KU Leuven, Belgium, for helpful discussions and training in experimental techniques.



- Franceschi C, Bonafè M, Valensin S, Olivieri F, De Luca M, Ottaviani E, De Benedictis G. 2000 Inflamm-aging. An evolutionary perspective on immunosenescence. *Ann. N. Y. Acad. Sci.* **908**, 244–254. (doi:10.1111/j.1749-6632.2000.tb06651.x)
- Prasad S, Sung B, Aggarwal BB. 2012 Age-associated chronic diseases require age-old medicine: role of chronic inflammation. *Prev. Med.* **54**, S29–S37. (doi:10.1016/j.ypmed.2011.11.011)
- Childs BG, Durik M, Baker DJ, Van Deursen JM. 2015 Cellular senescence in aging and age-related disease: from mechanisms to therapy. *Nat. Med.* **21**, 1424–1435. (doi:10.1038/nm.4000)
- Flatt T. 2012 A new definition of aging? *Front. Genet.* **3**, 148. (doi:10.3389/fgene.2012.00148)
- Chiao YA, Rabinovitch PS. 2015 The aging heart. *Cold Spring Harb. Perspect. Med.* **5**, a025148. (doi:10.1101/cshperspect.a025148)
- Vasto S *et al.* 2007 Inflammatory networks in ageing, age-related diseases and longevity. *Mech. Ageing Dev.* **128**, 83–91. (doi:10.1016/j.mad.2006.11.015)
- Wynn TA, Ramalingam TR. 2012 Mechanisms of fibrosis: therapeutic translation for fibrotic disease. *Nat. Med.* **18**, 1028–1040. (doi:10.1038/nm.2807)
- Wynn TA. 2008 Cellular and molecular mechanisms of fibrosis. *J. Pathol.* **214**, 199–210. (doi:10.1002/path.2277)
- Schuppan D, Ruehl M, Somasundaram R, Hahn EG. 2001 Matrix as a modulator of hepatic fibrogenesis. *Semin. Liver Dis.* **21**, 351–372. (doi:10.1055/s-2001-17556)
- Kryczka J, Boncela J. 2015 Leukocytes: the double-edged sword in fibrosis. *Mediat. Inflamm.* **2015**, 652035. (doi:10.1155/2015/652035)
- Lacy P. 2006 Mechanisms of degranulation in neutrophils. *Allergy Asthma Clin. Immunol.* **2**, 98–108. (doi:10.1186/1710-1492-2-3-98)
- Ackerman GA. 1971 The human neutrophilic promyelocyte. A correlated phase and electron microscopic study. *Z. Zellforsch. Mikrosk. Anat.* **118**, 467–481. (doi:10.1007/BF00324614)
- Clark RA. 1999 Activation of the neutrophil respiratory burst oxidase. *J. Infect. Dis.* **179**(Suppl 2), S309–S317. (doi:10.1086/513849)
- Metzler KD, Goosmann C, Lubojemska A, Zychlinsky A, Papayannopoulos V. 2014 A myeloperoxidase-containing complex regulates neutrophil elastase release and actin dynamics during NETosis. *Cell Rep.* **8**, 883–896. (doi:10.1016/j.celrep.2014.06.044)
- Papayannopoulos V, Metzler KD, Hakkim A, Zychlinsky A. 2010 Neutrophil elastase and myeloperoxidase regulate the formation of neutrophil extracellular traps. *J. Cell Biol.* **191**, 677–691. (doi:10.1083/jcb.201006052)
- Hakkim A, Fuchs TA, Martinez NE, Hess S, Prinz H, Zychlinsky A, Waldmann H. 2011 Activation of the Raf-MEK-ERK pathway is required for neutrophil extracellular trap formation. *Nat. Chem. Biol.* **7**, 75–77. (doi:10.1038/nchembio.496)
- Wang Y *et al.* 2004 Human PAD4 regulates histone arginine methylation levels via demethylation. *Science* **306**, 279–283. (doi:10.1126/science.1101400)
- Brinkmann V, Reichard U, Goosmann C, Fauler B, Uhlemann Y, Weiss DS, Weinrauch Y, Zychlinsky A. 2004 Neutrophil extracellular traps kill bacteria. *Science* **303**, 1532–1535. (doi:10.1126/science.1092385)
- Braian C, Hoge V, Stendahl O. 2013 *Mycobacterium tuberculosis*-induced neutrophil extracellular traps activate human macrophages. *J. Innate Immun.* **5**, 591–602. (doi:10.1159/000348676)
- Martinod K *et al.* 2017 Peptidylarginine deiminase 4 promotes age-related organ fibrosis. *J. Exp. Med.* **214**, 439–458. (doi:10.1084/jem.20160530)
- Fuchs TA *et al.* 2010 Extracellular DNA traps promote thrombosis. *Proc. Natl Acad. Sci. USA* **107**, 15 880–15 885. (doi:10.1073/pnas.1005743107)
- Demers M, Wagner DD. 2013 Neutrophil extracellular traps: a new link to cancer-associated thrombosis and potential implications for tumor progression. *Oncimmunology* **2**, e22946. (doi:10.4161/onci.22946)
- Martinod K, Wagner DD. 2014 Thrombosis: tangled up in NETs. *Blood* **123**, 2768–2776. (doi:10.1182/blood-2013-10-463646)
- Cools-Lartigue J, Spicer J, McDonald B, Gowing S, Chow S, Giannias B, Bourdeau F, Kubes P, Ferri L. 2013 Neutrophil extracellular traps sequester circulating tumor cells and promote metastasis. *J. Clin. Invest.* **123**, 3446–3458. (doi:10.1172/jci67484)
- Savchenko AS, Borissoff JI, Martinod K, De Meyer SF, Gallant M, Erpenbeck L, Brill A, Wang Y, Wagner DD. 2014 VWF-mediated leukocyte recruitment with chromatin decondensation by PAD4 increases myocardial ischemia/reperfusion injury in mice. *Blood* **123**, 141–148. (doi:10.1182/blood-2013-07-514992)
- Borissoff JI *et al.* 2013 Elevated levels of circulating DNA and chromatin are independently associated with severe coronary atherosclerosis and a prothrombotic state. *Arterioscler. Thromb. Vasc. Biol.* **33**, 2032–2040. (doi:10.1161/ATVBAHA.113.301627)
- Quillard T, Araújo HA, Franck G, Shvartz E, Sukhova G, Libby P. 2015 TLR2 and neutrophils potentiate endothelial stress, apoptosis and detachment: implications for superficial erosion. *Eur. Heart J.* **36**, 1394–1404. (doi:10.1093/eurheartj/ehv044)
- Warnatsch A, Ioannou M, Wang Q, Papayannopoulos V. 2015 Inflammation. Neutrophil extracellular traps license macrophages for cytokine production in atherosclerosis. *Science* **349**, 316–320. (doi:10.1126/science.aaa8064)
- Sur Chowdhury C, Giaglis S, Walker UA, Buser A, Hahn S, Hasler P. 2014 Enhanced neutrophil extracellular trap generation in rheumatoid arthritis: analysis of underlying signal transduction pathways and potential diagnostic utility. *Arthritis Res. Ther.* **16**, R122. (doi:10.1186/ar4579)
- Radic M, Marion TN. 2013 Neutrophil extracellular chromatin traps connect innate immune response to autoimmunity. *Semin. Immunopathol.* **35**, 465–480. (doi:10.1007/s00281-013-0376-6)
- Schindelin J *et al.* 2012 Fiji: an open-source platform for biological-image analysis. *Nat. Methods* **9**, 676–682. (doi:10.1038/nmeth.2019)
- Latif S, Bauer-Sardina I, Ranade K, Livak KJ, Kwok P-Y. 2001 Fluorescence polarization in homogeneous nucleic acid analysis II: 5'-nuclease assay. *Genome Res.* **11**, 436–440. (doi:10.1101/gr.156601)
- Martinod K, Demers M, Fuchs TA, Wong SL, Brill A, Gallant M, Hu J, Wang Y, Wagner DD. 2013 Neutrophil histone modification by peptidylarginine deiminase 4 is critical for deep vein thrombosis in mice. *Proc. Natl Acad. Sci. USA* **110**, 8674–8679. (doi:10.1073/pnas.1301059110)
- Li P, Li M, Lindberg MR, Kennett MJ, Xiong N, Wang Y. 2010 PAD4 is essential for antibacterial innate immunity mediated by neutrophil extracellular traps. *J. Exp. Med.* **207**, 1853–1862. (doi:10.1084/jem.20100239)
- Murtha LA *et al.* 2019 The role of pathological aging in cardiac and pulmonary fibrosis. *Ageing Dis.* **10**, 419–428. (doi:10.14336/AD.2018.0601)
- Dadgar SK, Tyagi SP. 1979 Importance of heart weight, weights of cardiac ventricles and left ventricle plus septum/right ventricle ratio in assessing cardiac hypertrophy. *Jpn. Heart J.* **20**, 63–73. (doi:10.1536/hj.20.63)
- Vinuela A, Brown AA, Buil A, Tsai P-C, Davies MN, Bell JT, Dermizakis ET, Spector TD, Small KS. 2018 Age-dependent changes in mean and variance of gene expression across tissues in a twin cohort. *Hum. Mol. Genet.* **27**, 732–741. (doi:10.1093/hmg/ddx424)
- Teo YV, Capri M, Morsiani C, Pizza G, Faria AMC, Franceschi C, Neretti N. 2019 Cell-free DNA as a biomarker of aging. *Ageing Cell* **18**, e12890. (doi:10.1111/accel.12890)
- Biernacka A, Frangogiannis NG. 2011 Aging and cardiac fibrosis. *Ageing Dis.* **2**, 158–173.
- ChandraRajan J. 1978 Separation of type III collagen from type I collagen and pepsin by differential denaturation and renaturation. *Biochem. Biophys. Res. Commun.* **83**, 180–186. (doi:10.1016/0006-291X(78)90414-X)
- Zhang G, Young BB, Ezura Y, Favata M, Soslowy LJ, Chakravarti S, Birk DE. 2005 Development of tendon structure and function: regulation of collagen fibrillogenesis. *J. Musculoskelet. Neuronal Interact.* **5**, 5–21.
- Birk DE, Mayne R. 1997 Localization of collagen types I, III and V during tendon development. Changes in collagen types I and III are correlated with changes in fibril diameter. *Eur. J. Cell Biol.* **72**, 352–361.

43. Fan D, Takawale A, Basu R, Patel V, Lee J, Kandalam V, Wang X, Oudit GY, Kassiri Z. 2014 Differential role of TIMP2 and TIMP3 in cardiac hypertrophy, fibrosis, and diastolic dysfunction. *Cardiovasc. Res.* **103**, 268–280. (doi:10.1093/cvr/cvu072)
44. Liu H, Jing X, Dong A, Bai B, Wang H. 2017 Overexpression of TIMP3 protects against cardiac ischemia/reperfusion injury by inhibiting myocardial apoptosis through ROS/Mapks pathway. *Cell. Physiol. Biochem.* **44**, 1011–1023. (doi:10.1159/000485401)
45. Fedak PW *et al.* 2004 TIMP-3 deficiency leads to dilated cardiomyopathy. *Circulation* **110**, 2401–2409. (doi:10.1161/01.CIR.0000134959.83967.2D)
46. Li H *et al.* 2000 MMP/TIMP expression in spontaneously hypertensive heart failure rats: the effect of ACE- and MMP-inhibition. *Cardiovasc. Res.* **46**, 298–306. (doi:10.1016/S0008-6363(00)00028-6)
47. Smith Jr GN, Mickler EA, Hasty KA, Brandt KD. 1999 Specificity of inhibition of matrix metalloproteinase activity by doxycycline: relationship to structure of the enzyme. *Arthritis Rheum.* **42**, 1140–1146. (doi:10.1002/1529-0131(199906)42:6<1140::AID-ANR10>3.0.CO;2-7)
48. Jaffré F, Friedman AE, Hu Z, Mackman N, Blaxall BC. 2012  $\beta$ -adrenergic receptor stimulation transactivates protease-activated receptor 1 via matrix metalloproteinase 13 in cardiac cells. *Circulation* **125**, 2993–3003. (doi:10.1161/CIRCULATIONAHA.111.066787)
49. Gullestad L, Ueland T, Vinge LE, Finsen A, Yndestad A, Aukrust P. 2012 Inflammatory cytokines in heart failure: mediators and markers. *Cardiology* **122**, 23–35. (doi:10.1159/000338166)
50. Reichel CA, Rehberg M, Lerchenberger M, Berberich N, Bihari P, Khandoga AG, Zahler S, Krombach F. 2009 Ccl2 and Ccl3 mediate neutrophil recruitment via induction of protein synthesis and generation of lipid mediators. *Arterioscler. Thromb. Vasc. Biol.* **29**, 1787–1793. (doi:10.1161/ATVBAHA.109.193268)
51. Moore BB, Murray L, Das A, Wilke CA, Herrygers AB, Toews GB. 2006 The role of CCL12 in the recruitment of fibrocytes and lung fibrosis. *Am. J. Respir. Cell Mol. Biol.* **35**, 175–181. (doi:10.1165/rcmb.2005-02390C)
52. Dorn LE, Petrosino JM, Wright P, Accornero F. 2018 CTGF/CCN2 is an autocrine regulator of cardiac fibrosis. *J. Mol. Cell. Cardiol.* **121**, 205–211. (doi:10.1016/j.yjmcc.2018.07.130)
53. Weng NP. 2006 Aging of the immune system: how much can the adaptive immune system adapt? *Immunity* **24**, 495–499. (doi:10.1016/j.immuni.2006.05.001)
54. Armstrong EJ, Morrow DA, Sabatine MS. 2006 Inflammatory biomarkers in acute coronary syndromes: part I: introduction and cytokines. *Circulation* **113**, e72–e75. (doi:10.1161/CIRCULATIONAHA.105.595520)
55. Markousis-Mavrogenis G *et al.* 2019 The clinical significance of interleukin-6 in heart failure: results from the BIOSTAT-CHF study. *Eur. J. Heart Fail* **21**, 965–973. (doi:10.1002/ehf.1482)
56. Wu CL, Yin R, Wang S-N, Ying R. 2021 A review of CXCL1 in cardiac fibrosis. *Front. Cardiovasc. Med.* **8**, 674498. (doi:10.3389/fcvm.2021.674498)
57. Sawant KV, Poluri KM, Dutta AK, Sepuru KM, Troshkina A, Garofalo RP, Rajarathnam K. 2016 Chemokine CXCL1 mediated neutrophil recruitment: role of glycosaminoglycan interactions. *Sci. Rep.* **6**, 33123. (doi:10.1038/srep33123)
58. De Filippo K, Henderson RB, Laschinger M, Hogg N. 2008 Neutrophil chemokines KC and macrophage-inflammatory protein-2 are newly synthesized by tissue macrophages using distinct TLR signaling pathways. *J. Immunol.* **180**, 4308–4315. (doi:10.4049/jimmunol.180.6.4308)
59. Zhang YL *et al.* 2019 Chronic inhibition of chemokine receptor CXCR2 attenuates cardiac remodeling and dysfunction in spontaneously hypertensive rats. *Biochim. Biophys. Acta Mol. Basis Dis.* **1865**, 165551. (doi:10.1016/j.bbdis.2019.165551)
60. Martinod K, Van Bruggen S. 2023 Replication Data for: Neutrophil peptidylarginine deiminase 4 is essential for detrimental age-related cardiac remodelling and dysfunction in mice. *KU Leuven RDR Research Data Repository.* (doi:10.48804/HCSSJE)
61. Van Bruggen S *et al.* 2023 Neutrophil peptidylarginine deiminase 4 is essential for detrimental age-related cardiac remodelling and dysfunction in mice. Figshare. (doi:10.6084/m9.figshare.c.6806584)